

## Thermodynamics of SU(3) gauge theory on anisotropic lattices

CP-PACS Collaboration : Y. Namekawa,<sup>a</sup> S. Aoki,<sup>a</sup> R. Burkhalter,<sup>a,b</sup> S. Ejiri,<sup>b</sup> M. Fukugita,<sup>c</sup> S. Hashimoto,<sup>d</sup>  
 N. Ishizuka,<sup>b</sup> Y. Iwasaki,<sup>a,b</sup> K. Kanaya,<sup>a</sup> T. Kaneko,<sup>d</sup> Y. Kuramashi,<sup>d</sup> V. Lesk,<sup>b</sup> M. Okamoto,<sup>b</sup> M. Okawa,<sup>d</sup>  
 Y. Taniguchi,<sup>a</sup> A. Ukawa,<sup>b</sup> and T. Yoshié<sup>b</sup>

<sup>a</sup>*Institute of Physics, University of Tsukuba, Tsukuba, Ibaraki 305-8571, Japan*

<sup>b</sup>*Center for Computational Physics, University of Tsukuba, Tsukuba, Ibaraki 305-8577, Japan*

<sup>c</sup>*Institute for Cosmic Ray Research, University of Tokyo, Kashiwa 277-8582, Japan*

<sup>d</sup>*High Energy Accelerator Research Organization (KEK), Tsukuba, Ibaraki 305-0801, Japan*

(November 19, 2018)

Finite temperature SU(3) gauge theory is studied on anisotropic lattices using the standard plaquette gauge action. The equation of state is calculated on  $16^3 \times 8$ ,  $20^3 \times 10$  and  $24^3 \times 12$  lattices with the anisotropy  $\xi \equiv a_s/a_t = 2$ , where  $a_s$  and  $a_t$  are the spatial and temporal lattice spacings. Unlike the case of the isotropic lattice on which  $N_t = 4$  data deviate significantly from the leading scaling behavior, the pressure and energy density on an anisotropic lattice are found to satisfy well the leading  $1/N_t^2$  scaling from our coarsest lattice,  $N_t/\xi = 4$ . With three data points at  $N_t/\xi = 4, 5$  and  $6$ , we perform a well controlled continuum extrapolation of the equation of state. Our results in the continuum limit agree with a previous result from isotropic lattices using the same action, but have smaller and more reliable errors.

11.15.Ha, 12.38.Gc, 12.38.Mh, 05.70.Ce

### I. INTRODUCTION

Study of lattice QCD at finite temperatures is an important step towards clarification of the dynamics of the quark gluon plasma which is believed to have formed in the early Universe and is expected to be created in high energy heavy ion collisions [1]. In order to extract predictions for the real world from results obtained on finite lattices, we have to extrapolate lattice data to the continuum limit of vanishing lattice spacings. Because of the large computational demands for full QCD simulations, continuum extrapolations of thermodynamic quantities have so far been attempted only in SU(3) gauge theory, *i.e.*, in the quenched approximation of QCD, where the influence of dynamical quarks is neglected. Two studies using the standard plaquette gauge action [2] and a renormalization-group (RG) improved gauge action [3] have found the pressure and energy density consistent with each other in the continuum limit.

In full QCD with two flavors of dynamical quarks, thermodynamic quantities on coarse lattices have been found to show large lattice spacing dependence [4–6]. For a reliable extrapolation to the continuum limit, data on finer lattices are required. With conventional isotropic lattices, this means an increase of the spatial lattice size to keep the physical volume close to the thermodynamic limit. Full QCD simulations on large lattices are still difficult with the current computer power. A more efficient method of calculation is desirable. Even in the quenched case, we note that continuum extrapolations of equation of state have been made using only two lattice spacings [2,3]. In order to reliably estimate systematic errors from the extrapolations, more data points are needed. Therefore, an efficient method is called for also in quenched QCD.

Recently, anisotropic lattices have been employed to study transport coefficients and temporal correlation functions in finite temperature QCD [7–9]. In these studies, anisotropy was introduced to obtain more data points for temporal correlation functions.

In this paper, we show that anisotropic lattices provide also an efficient calculation method for thermodynamic quantities. The idea is as follows. Inspecting the free energy density of SU(3) gauge theory in the high temperature Stephan-Boltzmann limit, the leading discretization error from the temporal direction is found to be much larger than that from each of the spatial directions. Hence, choosing  $\xi = a_s/a_t$  larger than one, where  $a_s$  and  $a_t$  are the spatial and temporal lattice spacings, cutoff errors in thermodynamic quantities will be efficiently reduced without much increase in the computational cost. From a study of free energy density in the high temperature limit, we find that  $\xi = 2$  is an optimal choice for SU(3) gauge theory. This improvement also makes it computationally easier to accumulate data for more values of temporal lattice sizes for the continuum extrapolation.

As a first test of the method, we study the equation of state (EOS) in SU(3) gauge theory. On isotropic lattices, discretization errors in the EOS for the plaquette action are quite large at the temporal lattice size  $N_t = 4$ . The data

at this value of  $N_t$  deviate significantly from the leading  $1/N_t^2$  scaling behavior,  $F(T)|_{N_t} = F(T)|_{\text{continuum}} + c_F/N_t^2$ , where  $F$  is a thermodynamic quantity at a fixed temperature  $T$ . So far, continuum extrapolations of the EOS have been made using results at  $N_t = 6$  and  $8$ . On anisotropic lattices with  $\xi = 2$ , we find that the discretization errors in the pressure and energy density are much reduced relative to those from isotropic lattices with the same spatial lattice spacing. Furthermore, we find that the EOS at  $N_t/\xi = 4, 5$  and  $6$  follow the leading  $1/N_t^2$  scaling behavior remarkably well. Therefore, a continuum extrapolation can be reliably carried out. Since the total computational cost is still lower than that for an  $N_t = 8$  isotropic simulation, we can achieve a higher statistics as well, resulting in smaller final errors.

In Sec. II, we study the high temperature limit of SU(3) gauge theory on anisotropic lattices to see how  $\xi$  appears in the leading discretization error for the EOS. From this study, we find that  $\xi = 2$  is an optimum choice for our purpose. We then perform a series of simulations on  $\xi = 2$  anisotropic lattices. Our lattice action and simulation parameters are described in Sec. III. Sec. IV is devoted to a calculation of the lattice scale through the string tension. The critical temperature is determined in Sec. V. Our main results are presented in Secs. VI and VII, where the pressure and energy density are calculated and their continuum extrapolations are carried out. A brief summary is given in Sec. VIII.

## II. HIGH TEMPERATURE LIMIT

In the high temperature limit, the gauge coupling vanishes due to asymptotic freedom, and SU(3) gauge theory turns into a free bosonic gas. In the integral method [10] which we apply in this study, the pressure  $p$  is related to the free energy density  $f$  by  $p = -f$  for large homogeneous systems. Therefore, in the high temperature limit, the energy density  $\epsilon$  is given by  $\epsilon = 3p = -3f$ . The value of  $f$  in the high temperature limit has been calculated in [11,12]. Normalizing  $\epsilon$  by the Stephan-Boltzmann value in the continuum limit, we find

$$\frac{\epsilon}{\epsilon_{SB}} = 1 + \frac{5 + 3\xi^2}{21} \left(\frac{\pi}{N_t}\right)^2 + \frac{91 + 210\xi^2 + 99\xi^4}{1680} \left(\frac{\pi}{N_t}\right)^4 + O\left(\left(\frac{\pi}{N_t}\right)^6\right) \quad (1)$$

for spatially large lattices. Substituting  $\xi = 1$  in Eq. (1), we recover the previous results for isotropic lattices [13]. When we alternatively adopt the derivative method (operator method) [11] to define the energy density, we obtain

$$\frac{\epsilon}{\epsilon_{SB}} = 1 + \frac{5(1 + \xi^2)}{21} \left(\frac{\pi}{N_t}\right)^2 + \frac{13 + 50\xi^2 + 33\xi^4}{240} \left(\frac{\pi}{N_t}\right)^4 + O\left(\left(\frac{\pi}{N_t}\right)^6\right). \quad (2)$$

In both formulae, the leading discretization error is proportional to  $1/N_t^2$ .

In the leading  $1/N_t^2$  term of Eq. (1) (or Eq. (2)), the term proportional to  $\xi^2$  represents the discretization error from finite lattice spacings  $a_s$  in the three spatial directions. We find that the temporal cutoff  $a_t$  leads to  $5/8$  (or  $1/2$ ) of the leading discretization error at  $\xi = 1$ , while the spatial cutoff  $a_s$  contributes only  $1/8$  (or  $1/6$ ) from each of the three spatial directions.

Since a reduction of the lattice spacing in each direction separately causes an increase of the computational cost by a similar magnitude, a reduction of  $a_t$  is much more efficient than that of  $a_s$  in suppressing lattice artifacts in thermodynamic quantities. Making the anisotropy  $\xi = a_s/a_t$  too large is, however, again inefficient because the spatial discretization errors remain even in the limit of  $\xi = \infty$ . A rough estimate for the optimum value of  $\xi$  is given by equating the discretization errors from spatial and temporal directions,  $\xi = \sqrt{5} \approx 2.24$  from Eq. (1), and  $\xi = \sqrt{3} \approx 1.73$  from Eq. (2). More elaborate estimations considering the balance between the computational cost as a function of the lattice size and the magnitude of discretization errors including higher orders of  $1/N_t$  lead to similar values of  $\xi$ .

Based on these considerations, we adopt  $\xi = 2$  for simulations of SU(3) gauge theory in the present work. An even number for  $\xi$  is attractive also for the vectorization/parallelization of the simulation code which is based on an even-odd algorithm, since we can study the case of odd  $N_t/\xi$  without modifying the program.

## III. DETAILS OF SIMULATIONS

### A. Action

We employ the plaquette gauge action for SU(3) gauge theory given by

$$S_G[U] = \beta \left( \frac{1}{\xi_0} Q_s + \xi_0 Q_t \right), \quad (3)$$

where  $\xi_0$  is the bare anisotropy,  $\beta = 6/g_0^2$  with  $g_0$  the bare gauge coupling constant, and

$$Q_s = \sum_{n,(ij)} (1 - P_{ij}(n)), \quad Q_t = \sum_{n,i} (1 - P_{i4}(n)), \quad (4)$$

with  $P_{\mu\nu}(n) = \frac{1}{3} \text{Re Tr } U_{\mu\nu}(n)$  the plaquette in the  $(\mu, \nu)$  plane at site  $n$ . Anisotropy is introduced by choosing  $\xi_0 \neq 1$ .

Due to quantum fluctuations, the actual anisotropy  $\xi \equiv a_s/a_t$  deviates from the bare value  $\xi_0$ . We define the renormalization factor  $\eta(\beta, \xi)$  for  $\xi$  by

$$\eta(\beta, \xi) = \frac{\xi}{\xi_0(\beta, \xi)}. \quad (5)$$

The values of  $\eta(\beta, \xi)$  can be determined non-perturbatively by matching Wilson loops in temporal and spatial directions on anisotropic lattices [13–16]. For our simulation, we calculate  $\xi_0(\beta, \xi = 2)$  using  $\eta(\beta, \xi)$  obtained by Klassen for the range  $1 \leq \xi \leq 6$  and  $5.5 \leq \beta \leq \infty$  [16]:

$$\eta(\beta, \xi) = 1 + \left( 1 - \frac{1}{\xi} \right) \frac{\hat{\eta}_1(\xi)}{6} \frac{1 + a_1 g_0^2}{1 + a_0 g_0^2} g_0^2, \quad (6)$$

where  $a_0 = -0.77810$ ,  $a_1 = -0.55055$  and

$$\hat{\eta}_1(\xi) = \frac{1.002503\xi^3 + 0.39100\xi^2 + 1.47130\xi - 0.19231}{\xi^3 + 0.26287\xi^2 + 1.59008\xi - 0.18224}. \quad (7)$$

## B. Simulation parameters

The main runs of our simulations are carried out on  $\xi = 2$  anisotropic lattices with size  $N_s^3 \times N_t = 16^3 \times 8$ ,  $20^3 \times 10$  and  $24^3 \times 12$ . For  $N_t = 8$ , we make additional runs on  $12^3 \times 8$  and  $24^3 \times 8$  lattices to examine finite size effects. The zero-temperature runs are made on  $N_s^3 \times \xi N_s$  lattices with  $\xi = 2$ . The simulation parameters of these runs which cover the range  $T/T_c \sim 0.9$ – $5.0$  are listed in Table I. To determine precise values for the critical coupling, longer runs around the critical points are made at the parameters compiled in Table II.

For the main runs, the aspect ratio  $L_s T = (N_s a_s)/(N_t a_t)$  is fixed to 4, where  $L_s = N_s a_s$  is the spatial lattice size in physical units. This choice is based on a study of finite spatial volume effects presented in Sec. VI, where it is shown that, for the precision and the range of  $T/T_c$  we study, finite spatial volume effects in the EOS are sufficiently small with  $L_s T \geq 4$ .

Gauge configurations are generated by a 5-hit pseudo heat bath update followed by four over-relaxation sweeps, which we call an iteration. As discussed in Sec. VI, the total number of iterations should be approximately proportional to  $N_t^6$  to keep an accuracy for the EOS. After thermalization, we perform 20,000 to 100,000 iterations on finite-temperature lattices and 5,000 to 25,000 iterations on zero-temperature lattices, as compiled in Table I. At every iteration, we measure the spatial and temporal plaquettes,  $P_{ss}$  and  $P_{st}$ . Near the critical temperature, we also measure the Polyakov loop. The errors are estimated by a jack-knife method. The bin size for the jack-knife errors, listed in Table I, is determined from a study of bin size dependence as illustrated in Fig. 1. The results for the plaquettes are summarized in Tables III–V.

## IV. SCALE

### A. Static quark potential

We determine the physical scale of our lattices from the string tension, which is calculated from the static quark-antiquark potential at zero temperature. To calculate the static quark potential, we perform additional zero-temperature simulations listed in Table VI. The static quark potential  $V(\hat{R})$  is defined through

$$W(\hat{R}, \hat{T}) = C(\hat{R}) e^{-V(\hat{R})\hat{T}/\xi}, \quad (8)$$

where  $W(\hat{R}, \hat{T})$  is the Wilson loop in a spatial-temporal plane with the size  $\hat{R}a_s \times \hat{T}a_t$ . We measure Wilson loops at every 25 iterations after thermalization. In order to enhance the ground state signal in (8), we smear the spatial links of the Wilson loop [17,18]. Details of the smearing method are the same as in Ref. [19]. We determine the optimum smearing step  $N_{opt}$  which maximizes the overlap function  $C(\hat{R})$  under the condition  $C(\hat{R}) \leq 1$ . Following Ref. [18], we study a local effective potential defined by

$$V_{eff}(\hat{R}, \hat{T}) = \xi \log \left( \frac{W(\hat{R}, \hat{T})}{W(\hat{R}, \hat{T} + 1)} \right), \quad (9)$$

which tends to  $V(\hat{R})$  at sufficiently large  $\hat{T}$ . The reason to adopt Eq. (9) instead of the fit result from Eq. (8) is to perform a correlated error analysis directly for the potential parameters. The optimum value of  $\hat{T}$ , listed in Table VII, is obtained by inspecting the plateau of  $V_{eff}(\hat{R}, \hat{T})$  at each  $\beta$ .

We perform a correlated fit of  $V(\hat{R}) = V_{eff}(\hat{R}, \hat{T}_{opt})$  with the ansatz [20],

$$V(\hat{R}) = V_0 + \sigma \hat{R} - e \frac{1}{\hat{R}} + l \left( \frac{1}{\hat{R}} - \left[ \frac{1}{\hat{R}} \right] \right). \quad (10)$$

Here,  $\left[ \frac{1}{\hat{R}} \right]$  is the lattice Coulomb term from one gluon exchange

$$\left[ \frac{1}{\hat{R}} \right] = 4\pi \int_{-\pi}^{\pi} \frac{d^3 \mathbf{k}}{(2\pi)^3} \frac{\cos(\mathbf{k} \cdot \hat{\mathbf{R}})}{4 \sum_{i=1}^3 \sin^2(k_i a_s / 2)}, \quad (11)$$

which is introduced to approximately remove terms violating rotational invariance at short distances. The coefficient  $l$  is treated as a free parameter.

The fit range  $[\hat{R}_{min}, \hat{R}_{max}]$  for  $\hat{R}$  is determined by consulting the stability of the fit. Our choices for  $\hat{R}_{min}$  are given in Table VII. We confirm that the fits and the values of the string tension are stable under a variation of  $\hat{R}_{min}$ . The string tension is almost insensitive to a wide variation of  $\hat{R}_{max}$ . Hence  $\hat{R}_{max}$  is chosen as large as possible so far as the fit is stable and the signal is not lost in the noise. With this choice for the fit range, we obtain fit curves which reproduce the data well.

Our results for the potential parameters are summarized in Table VII. The error includes the jack-knife error with bin size one (25 iterations) and the systematic error from the choice of  $\hat{R}_{min}$  estimated through a difference under the change of  $\hat{R}_{min}$  by one. We confirm that increasing the bin size to two gives consistent results on  $16^3 \times 32$  lattices, while, on  $24^3 \times 48$  lattices, correlated fits with bin size two become unstable due to insufficient number of jackknife ensembles.

## B. String tension

We interpolate the string tension data using an ansatz proposed by Allton [21],

$$a_s \sqrt{\sigma} = f(\beta) \frac{1 + c_2 \hat{a}(\beta)^2 + c_4 \hat{a}(\beta)^4}{c_0}, \quad (12)$$

where  $f(\beta)$  is the two-loop scaling function of SU(3) gauge theory,

$$f(\beta) = \left( \frac{6b_0}{\beta} \right)^{-\frac{b_1}{2b_0^2}} \exp\left[-\frac{\beta}{12b_0}\right],$$

$$b_0 = \frac{11}{16\pi^2}, \quad b_1 = \frac{102}{(16\pi^2)^2}, \quad (13)$$

and  $\hat{a}(\beta) \equiv f(\beta)/f(\beta = 6.0)$ .

From Table VII, we find that the values for  $a_s \sqrt{\sigma}$  are insensitive to the spatial lattice volume to the present precision. Using data marked by star (\*) in Table VII, we obtain the best fit at

$$c_0 = 0.01171(41), \quad c_2 = 0.285(79), \quad c_4 = 0.033(30), \quad (14)$$

with  $\chi^2/N_{DF} = 1.77$ . The string tension data and the resulting fit curve are shown in Fig. 2, together with those from isotropic lattices [22].

## V. CRITICAL TEMPERATURE

We define the critical gauge coupling  $\beta_c(N_t, N_s)$  from the location of the peak of the susceptibility  $\chi_{rot}$  for a Z(3)-rotated Polyakov loop. The simulation parameters for the study of  $\beta_c$  are compiled in Table II. The  $\beta$ -dependence of  $\chi_{rot}$  is calculated using the spectral density method [23]. The results for  $\beta_c$  are compiled in Table VIII.

To estimate the critical temperature, we have to extrapolate  $\beta_c(N_t, N_s)$  to the thermodynamic limit and to the continuum limit. We perform the extrapolation to the thermodynamic limit using a finite-size scaling ansatz,

$$\beta_c(N_t, N_s) = \beta_c(N_t, \infty) - h \left( \frac{N_t}{\xi N_s} \right)^3. \quad (15)$$

for first order phase transitions. From the data for  $\beta_c$  on anisotropic  $12^3 \times 8$ ,  $16^3 \times 8$  and  $24^3 \times 8$  lattices with  $\xi = 2$ , we find  $h = 0.031(16)$  for  $N_t/\xi = 4$ , as shown in Fig. 3. In a previous study on isotropic lattices,  $h$  was found to be approximately independent of  $N_t$  for  $N_t = 4$  and 6 [24]. We extract  $\beta_c(N_t, \infty)$  adopting  $h = 0.031(16)$  for all  $N_t$ .

The critical temperature in units of the string tension is given by

$$\frac{T_c}{\sqrt{\sigma}} = \frac{\xi}{N_t (a_s \sqrt{\sigma}) (\beta_c(N_t, \infty))} \quad (16)$$

using the fit result for Eq. (12). The values of  $T_c/\sqrt{\sigma}$  are summarized in Fig. 4 and Table VIII. The dominant part of the errors in  $T_c/\sqrt{\sigma}$  is from the Allton fit for the string tension.

Finally we extrapolate the results to the continuum limit assuming the leading  $1/N_t^2$  scaling ansatz,

$$F|_{N_t} = F|_{\text{continuum}} + \frac{cF}{N_t^2} \quad (17)$$

with  $F = T_c/\sqrt{\sigma}$ . The extrapolation is shown in Fig. 4. In the continuum limit, we obtain

$$\frac{T_c}{\sqrt{\sigma}} = 0.635(10) \quad (18)$$

from the  $\xi = 2$  plaquette action.

In Fig. 4, we also plot the results obtained on isotropic lattices using the plaquette action [25] and the RG-improved action [26,3]. Our value of  $T_c/\sqrt{\sigma}$  in the continuum limit is consistent with these results within the error of about 2%. A more precise comparison would require the generation and analyses of potential data in a completely parallel manner, because, as discussed in [3], numerical values of  $T_c/\sqrt{\sigma}$  at a few percent level sensitively depend on the method used to determine the string tension. We leave this issue for future studies.

## VI. PRESSURE

### A. Integral method

We use the integral method to calculate the pressure [10]. This method is based on the relation  $p = -f \equiv (T/V) \log Z(T, V)$  satisfied for a large homogeneous system, where  $V = L_s^3$  is the spatial volume of the system in physical units and  $Z$  is the partition function. Rewriting  $\log Z = \int d\beta \frac{1}{Z} \frac{\partial Z}{\partial \beta}$ , the pressure is given by

$$\frac{p}{T^4} \Big|_{\beta_0}^{\beta} = \int_{\beta_0}^{\beta} d\beta' \Delta S(\beta'), \quad (19)$$

with

$$\Delta S(\beta) \equiv \xi \left( \frac{N_t}{\xi} \right)^4 \frac{1}{N_s^3 N_t} \frac{\partial \log Z}{\partial \beta} \Big|_{\xi}. \quad (20)$$

For our anisotropic gauge action (3), the derivative of  $\log Z$  is given by

$$-\frac{\partial \log Z}{\partial \beta} = \left\langle \frac{S_G}{\beta} \right\rangle + \beta \frac{\partial \xi_0(\beta, \xi)}{\partial \beta} \left( \langle Q_t \rangle - \frac{\langle Q_s \rangle}{\xi_0^2(\beta, \xi)} \right) - (T = 0 \text{ contribution}). \quad (21)$$

We use symmetric  $N_s^3 \times \xi N_s$  lattices to calculate the  $T = 0$  contribution. For a sufficiently small  $\beta_0$ ,  $p(\beta_0)$  can be neglected.

In order to keep the same accuracy of  $\Delta S$  for the same physical lattice volume  $L_s^3$  in units of the temperature  $T$ , the statistics of simulations should increase in proportion to  $(\xi(N_t/\xi)^4)^2/(N_s^3 N_t) \propto N_t^4/\xi^3$ . Here, the first factor arises from  $\xi(N_t/\xi)^4$  in Eq. (20), and the second factor  $1/(N_s^3 N_t)$  from a suppression of fluctuations due to averaging over the lattice volume. Taking into account the autocorrelation time which is proportional to  $N_t^2$ , the number of iterations should increase as  $\sim N_t^6$ .

Integrating  $\Delta S$  in  $\beta$  using a cubic spline interpolation, we obtain the pressure. For the horizontal axis, we use the temperature in units of the critical temperature,

$$\frac{T}{T_c} = \frac{(a_s \sqrt{\sigma})(\beta_c)}{(a_s \sqrt{\sigma})(\beta)}. \quad (22)$$

The errors from numerical integration are estimated by a jack-knife method in the following way [3]. Since simulations at different  $\beta$  are statistically independent, we sum up all the contributions from  $\beta_i$  smaller than  $\beta$  corresponding to the temperature  $T$  by the naive error-propagation rule,  $\delta p(T) = \sqrt{\sum_i \delta p_i(T)^2}$ , where  $\delta_i p(T)$  at each simulation point  $\beta_i$  is estimated by the jack-knife method.

### B. Finite spatial volume effects

We first study the effects of finite spatial volume on the EOS. In Fig. 5, we show the results for  $\Delta S$  at  $N_t/\xi = 8/2$  with the aspect ratio  $L_s T = N_s \xi / N_t = 3, 4$  and  $6$  which correspond to  $N_s = 12, 16$  and  $24$ , respectively. Integrating  $\Delta S$  in  $\beta$ , we obtain Fig. 6 for the pressure. We find that the data at  $L_s T = 3$  is affected by sizable finite volume effects both at  $T \sim T_c$  and at high temperatures. On the other hand, for the range of  $T/T_c$  we study, the pressure does not change when the aspect ratio is increased from  $L_s T = 4$  to  $6$ , indicating that the conventional choice  $L_s T = 4$  is safe with the present precision of data. Hence, we choose  $L_s T = 4$  for our studies of lattice spacing dependence. Results for  $\Delta S$  at  $L_s T = 4$  with various  $N_t$  are given in Fig. 7. Integrating the data using a cubic spline interpolation, as shown in the figures, we obtain the pressure plotted in Fig. 8.

### C. Continuum extrapolation

We now extrapolate the pressure to the continuum limit using the leading order ansatz of Eq. (17). Figure 9 shows the pressure at  $T/T_c = 1.5, 2.5$  and  $3.5$  as a function of  $(\xi/N_t)^2$  (filled circles). For comparison, results from isotropic lattices using the plaquette action [2] (open circles) and the RG-improved action [3] (open squares) are also plotted. For the  $\xi = 1$  plaquette data, we adopt the results of a reanalysis made in Ref. [3] to commonly apply the scale from the Allton fit of the string tension and also the same error estimation method.

The advantage of using anisotropic lattices is apparent from Fig. 9. On the coarsest lattice  $N_t/\xi = 4$ , finite lattice spacing errors at  $\xi = 2$  are much smaller than those at  $\xi = 1$  with the same plaquette action. The pressure at  $T = 2.5T_c$ , for example, on the isotropic  $16^3 \times 4$  lattice is larger than its continuum limit by about 20%, while the deviation is only 5% on the corresponding  $16^3 \times 8$  lattice with  $\xi = 2$ . Furthermore, with the anisotropic  $\xi = 2$  data, the leading  $1/N_t^2$  term describes the data well even at  $N_t/\xi = 4$  (the right-most point). Therefore, we can confidently perform an extrapolation to the continuum limit using three data points. In the case of the isotropic plaquette action, in contrast, the continuum extrapolation had to be made with only two data points at  $N_t/\xi = 6$  and  $8$ . In the continuum limit, our results for  $\xi = 2$  are slightly smaller than those from the isotropic plaquette action, but the results are consistent with each other within the error of about 5% for the results from the isotropic action. It is worth observing that the  $\xi = 2$  results have smaller and more reliable errors of 2–3%.

In order to quantitatively evaluate the benefit of anisotropic lattices, we compare the computational cost to achieve comparable systematic and statistical errors on isotropic and  $\xi = 2$  anisotropic lattices. Choosing  $T = 2.5T_c$  as a typical example, we find that the deviation of the pressure from the continuum limit (*i.e.*, the magnitude of the systematic error due to finite lattice cutoffs) is comparable between the isotropic  $32^3 \times 8$  [2] and our  $\xi = 2$  anisotropic  $20^3 \times 10$  lattices, *i.e.*,  $p/T^4 = 1.390(26)$  on a  $32^3 \times 8$  lattice and  $p/T^4 = 1.381(13)$  on a  $20^3 \times 10$  lattice, both lattices having the same spatial size  $N_s a_s = 1.6/T_c$ . The number of configurations to achieve these statistical errors are 20,000–40,000 iterations for  $\xi = 1$  and 50,000 for  $\xi = 2$ , respectively. Therefore, for the same statistical error, the relative computational cost for a  $\xi = 2$  lattice over that for  $\xi = 1$  is conservatively estimated as  $((20^3 \times 10) \times 50000) / ((32^3 \times 8) \times 4 \times 20000) \approx 1/5$ , showing a factor 5 gain in the computational cost for the anisotropic calculation in this example.

In Fig. 9 we also note that the results from the RG-improved action on isotropic lattices are higher by 7–10% (about  $2\sigma$ ) than those from the present work in the continuum limit. A possible origin of this discrepancy is the use of the  $N_t/\xi = 4$  data of the RG-improved action, which show a large (about 20%) deviation from the continuum value. For a detailed test of consistency, we need more data points, say at  $N_t/\xi = 6$ , from the RG-improved action.

Repeating the continuum extrapolation at other values of  $T/T_c$ , we obtain Fig. 10. Our results show a quite slow approach to the high temperature Stephan-Boltzmann limit, as reported also in previous studies on isotropic lattices [2,3].

## VII. ENERGY DENSITY

We calculate the energy density  $\epsilon$  by combining the results of  $p/T^4$  with those for the interaction measure defined by

$$\frac{\epsilon - 3p}{T^4} = -a_s \left. \frac{\partial \beta}{\partial a_s} \right|_{\xi} \Delta S. \quad (23)$$

The QCD beta function on anisotropic lattice  $\left. \frac{\partial \beta}{\partial a_s} \right|_{\xi}$  is determined through the string tension  $\sigma$  studied in Sec. IV B,

$$a_s \left. \frac{\partial \beta}{\partial a_s} \right|_{\xi} = \frac{12b_0}{6(b_1/b_0)\beta^{-1} - 1} \frac{1 + c_2\hat{a}^2 + c_4\hat{a}^4}{1 + 3c_2\hat{a}^2 + 5c_4\hat{a}^4}, \quad (24)$$

where the coefficients  $c_i$  are given in Eq. (12). The error of the energy density is calculated by quadrature from the error of  $3p$  and that for  $\epsilon - 3p$ , the latter being proportional to the error of  $\Delta S$ .

The results for the energy density are shown in Figs. 11 and 12. As in the case of the pressure the leading scaling behavior is well followed by our  $\xi = 2$  data from  $N_t/\xi = 4$ , which allows us to extrapolate to the continuum limit reliably. The results for the energy density in the continuum limit are compared with the previous results in Fig. 13. Our  $\xi = 2$  plaquette action leads to an energy density which is slightly smaller than, but consistent with that from the  $\xi = 1$  plaquette action, but is about 7–10% (about  $2\sigma$ ) smaller than that from the  $\xi = 1$  RG action. More work is required to clarify the origin of the small discrepancy with the RG action.

## VIII. CONCLUSION

We have studied the continuum limit of the equation of state in SU(3) gauge theory on anisotropic lattices with the anisotropy  $\xi \equiv a_s/a_t = 2$ , using the standard plaquette gauge action. Anisotropic lattices are shown to be more efficient in calculating thermodynamic quantities than isotropic lattices. We found that the cutoff errors in the pressure and energy density are much smaller than corresponding isotropic lattice results at small values of  $N_t/\xi$ . The computational cost for  $\xi = 2$  lattices is about 1/5 of that for  $\xi = 1$  lattices. We also found that the leading scaling behavior is well satisfied already from  $N_t/\xi = 4$ , which enabled us to perform continuum extrapolations with three data points at  $N_t/\xi = 4, 5$  and 6. The equation of state in the continuum limit agrees with that obtained on isotropic lattice using the same action, but have much smaller and better controlled errors. The benefit of anisotropic lattice demonstrated here will be indispensable for extraction of continuum predictions for the equation of state, when we include dynamical quarks.

## ACKNOWLEDGEMENTS

This work is supported in part by Grants-in-Aid of the Ministry of Education (Nos. 10640246, 10640248, 11640250, 11640294, 12014202, 12304011, 12640253, 12740133, 13640260). SE and M. Okamoto are JSPS Research Fellows. VL is supported by the Research for Future Program of JSPS (No. JSPS-RFTF 97P01102). Simulations were performed on the parallel computer CP-PACS at the Center for Computational Physics, University of Tsukuba.

- [1] For a recent review, see S. Ejiri, Nucl. Phys. **B** (Proc. Suppl.) 94 (2001) 19.
- [2] G. Boyd *et al.*, Nucl. Phys. **B469** (1996) 419.
- [3] CP-PACS Collaboration: M. Okamoto *et al.*, Phys. Rev. **D60** (1999) 094510.
- [4] C. Bernard *et al.*, Phys. Rev. **D55** (1997) 6861.
- [5] J. Engels *et al.*, Phys. Lett. **B396** (1997) 210. F. Karsch, E. Laermann and A. Peikert, Phys. Lett. **B478** (2000) 447.
- [6] CP-PACS Collaboration: A. Ali Khan *et al.*, Phys. Rev. **D63** (2001) 034502; hep-lat/0102038.
- [7] S. Sakai, A. Nakamura and T. Saito, Nucl. Phys. **A638** (1998) 535.
- [8] QCD-TARO Collaboration: Ph. de Forcrand *et al.*, Phys. Rev. **D63** (2001) 054501.
- [9] T. Umeda, R. Katayama, O. Miyamura and H. Matsufuru, Nucl. Phys. **B** (Proc. Suppl.) **94** (2001) 435; hep-lat/0011085.
- [10] J. Engels, J. Fingberg, F. Karsch, D. Miller and M. Weber, Phys. Lett. **B252** (1990) 625.
- [11] J. Engels, F. Karsch and H. Satz, Nucl. Phys. **B205** (1982) 239.
- [12] H.-Th. Elze, K. Kajantie and J. Kapusta, Nucl. Phys. **B304** (1988) 832.
- [13] J. Engels, F. Karsch and T. Scheideler, Nucl. Phys. **B564** (2000) 303.
- [14] G. Burgers *et al.*, Nucl. Phys. **B304** (1988) 587.
- [15] QCD-TARO Collaboration: M. Fujisaki *et al.*, Nucl. Phys. **B**(Proc.Suppl.)**53** (1997) 426.
- [16] T.R. Klassen, Nucl. Phys. **B533** (1998) 557.
- [17] G.S. Bali and K. Schilling, Phys. Rev. **D46** (1992) 2636.
- [18] G.S. Bali and K. Schilling, Phys. Rev. **D47** (1993) 661.
- [19] CP-PACS Collaboration: A. Ali Khan *et al.*, Phys. Rev. **D60** (1999) 114508.
- [20] C. Michael, Phys. Lett. **B283** (1992) 103.
- [21] C. Allton, hep-lat/9610016.
- [22] R.G. Edwards, U.M. Heller, T.R. Klassen, Phys. Rev. Lett. **80** (1998) 3448.
- [23] I.R. McDonald and K. Singer, Discuss. Faraday Soc. **43** (1967) 40,  
A.M. Ferrenberg and R.H. Swendsen, Phys. Rev. Lett. **61** (1988) 2635; **63** (1989) 1195,  
S. Huang, K.J.M. Moriarty, E. Myers and J. Potvin, Z. Phys. **C50** (1991) 221.
- [24] Y. Iwasaki *et al.*, Phys. Rev. **D46** (1992) 4657.
- [25] B. Beinlich, F. Karsch, E. Laermann and A. Peikert, Eur. Phys. J. **C6** (1999) 133.
- [26] Y. Iwasaki, K. Kanaya, T. Kaneko and T. Yoshié, Phys. Rev. **D56** (1997) 151.



lattice	$\beta$	bin size	# of iter.
$12^3 \times 8$	5.73–6.80	1600	40 000
$16^3 \times 8^*$	5.74–6.80	800	20 000
$24^3 \times 8$	5.75–6.80	400	10 000
$20^3 \times 10^*$	5.86–6.98	2000	50 000
$24^3 \times 12^*$	5.95–7.20	4000	100 000
$12^3 \times 24$	5.74–6.80	400	10 000
$16^3 \times 32^*$	5.74–6.80	200	5 000
$20^3 \times 40^*$	5.86–6.98	500	12 500
$24^3 \times 48$	5.75–5.90	100	2 500
$24^3 \times 48^*$	5.95–7.20	1000	25 000

TABLE I. Simulation parameters. Main runs are marked by star (\*).

lattice	$\beta$	bin size	# of iter.
$12^3 \times 8$	5.790, 5.791	8000	80 000
$16^3 \times 8$	5.790, 5.792	4000	40 000
$24^3 \times 8$	5.791, 5.792	4000	40 000
$20^3 \times 10$	5.903, 5.907	5000	50 000
$24^3 \times 12$	6.004, 6.006	10000	100 000

TABLE II. Simulation parameters for determination of critical couplings.

$\beta$	$\xi_0$	$16^3 \times 8$		$16^3 \times 32$	
		$P_{ss}$	$P_{st}$	$P_{ss}$	$P_{st}$
5.740	1.66279318	0.448467(31)	0.679985(12)	0.448490(28)	0.679979(11)
5.750	1.66473308	0.450693(24)	0.681412(11)	0.450641(21)	0.681384(8)
5.760	1.66664410	0.452784(33)	0.682783(13)	0.452731(22)	0.682747(9)
5.770	1.66852693	0.454935(29)	0.684175(13)	0.454758(24)	0.684090(9)
5.780	1.67038223	0.457024(53)	0.685533(22)	0.456720(21)	0.685392(8)
5.788	1.67184708	0.459186(116)	0.686823(49)	0.458272(30)	0.686419(11)
5.790	1.67221065	0.459930(109)	0.687240(48)	0.458678(26)	0.686679(11)
5.792	1.67257316	0.460517(104)	0.687578(45)	0.459056(22)	0.686929(9)
5.800	1.67401280	0.462698(75)	0.688873(33)	0.460586(22)	0.687949(9)
5.805	1.67490422	0.463825(34)	0.689587(15)	0.461565(21)	0.688588(9)
5.810	1.67578929	0.464912(40)	0.690278(17)	0.462446(20)	0.689181(9)
5.820	1.67754071	0.466746(21)	0.691520(10)	0.464241(17)	0.690383(6)
5.830	1.67926762	0.468486(24)	0.692704(10)	0.466022(21)	0.691578(9)
5.840	1.68097058	0.470122(18)	0.693839(8)	0.467707(24)	0.692722(9)
5.880	1.68755324	0.476195(15)	0.698142(7)	0.474205(17)	0.697145(7)
5.900	1.69071395	0.478994(18)	0.700156(9)	0.477282(22)	0.699255(9)
5.950	1.69826359	0.485606(15)	0.704933(7)	0.484390(18)	0.704199(7)
6.000	1.70535029	0.491774(15)	0.709406(6)	0.490955(20)	0.708801(9)
6.100	1.71830738	0.503237(14)	0.717652(6)	0.502986(14)	0.717230(5)
6.200	1.72987892	0.513833(11)	0.725175(6)	0.513839(14)	0.724837(5)
6.300	1.74029271	0.523743(10)	0.732106(4)	0.523915(15)	0.731827(7)
6.400	1.74972820	0.533075(11)	0.738552(4)	0.533401(9)	0.738316(3)
6.500	1.75832876	0.541970(13)	0.744586(5)	0.542362(8)	0.744378(5)
6.600	1.76621035	0.550391(8)	0.750250(3)	0.550854(10)	0.750058(4)
6.700	1.77346785	0.558485(9)	0.755608(4)	0.558959(9)	0.755427(4)
6.800	1.78017964	0.566215(12)	0.760672(4)	0.566716(8)	0.760501(4)

TABLE III. Plaquette expectation values on  $16^3 \times 8$  and  $16^3 \times 32$  lattices with  $\xi = 2$ .

$\beta$	$\xi_0$	$20^3 \times 10$		$20^3 \times 40$	
		$P_{ss}$	$P_{st}$	$P_{ss}$	$P_{st}$
5.86288916	1.68478116	0.4715286(90)	0.6953072(38)	0.4715194(98)	0.6953039(38)
5.87	1.68594094	0.4726803(97)	0.6960907(37)	0.4726453(79)	0.6960771(33)
5.88583578	1.68848420	0.4752043(113)	0.6978062(52)	0.4751072(93)	0.6977655(41)
5.90	1.69071395	0.4775533(342)	0.6993698(144)	0.4772612(79)	0.6992430(33)
5.91	1.69226327	0.4793349(340)	0.7005240(144)	0.4787235(65)	0.7002573(30)
5.92	1.69379248	0.4809915(113)	0.7016191(50)	0.4801832(57)	0.7012665(26)
5.93084722	1.69542899	0.4826008(89)	0.7027227(39)	0.4817182(78)	0.7023359(35)
5.94	1.69679224	0.4838962(61)	0.7036250(30)	0.4830113(60)	0.7032314(30)
5.96	1.69971645	0.4865820(62)	0.7055225(30)	0.4857427(62)	0.7051382(32)
5.98	1.70256818	0.4891795(54)	0.7073650(25)	0.4883883(83)	0.7069900(34)
5.9961937	1.70482605	0.4912217(55)	0.7088160(30)	0.4904832(71)	0.7084591(30)
6.0793640	1.71575557	0.5010417(44)	0.7158270(31)	0.5005840(62)	0.7155576(27)
6.17716193	1.72734556	0.5116532(54)	0.7233550(25)	0.5114357(43)	0.7231598(22)
6.28582916	1.73888020	0.5225991(56)	0.7310157(21)	0.5225280(53)	0.7308687(21)
6.40118969	1.74983517	0.5334631(32)	0.7385009(19)	0.5334926(43)	0.7383839(17)
6.51881026	1.75986308	0.5438681(48)	0.7455581(19)	0.5439702(40)	0.7454657(19)
6.63417079	1.76875624	0.5535144(38)	0.7520032(19)	0.5536476(51)	0.7519204(23)
6.74283803	1.77640579	0.5621461(45)	0.7576970(23)	0.5623098(36)	0.7576251(14)
6.84063596	1.78276647	0.5695876(32)	0.7625475(17)	0.5697626(34)	0.7624799(11)
6.92380626	1.78783002	0.5756793(33)	0.7664882(18)	0.5758587(31)	0.7664206(16)
6.98915275	1.79160648	0.5803248(35)	0.7694702(14)	0.5805094(41)	0.7694057(18)

TABLE IV. Plaquette expectation values on  $20^3 \times 10$  and  $20^3 \times 40$  lattices with  $\xi = 2$ .

$\beta$	$\xi_0$	$24^3 \times 12$		$24^3 \times 48$	
		$P_{ss}$	$P_{st}$	$P_{ss}$	$P_{st}$
5.95	1.69826359	0.4843851(27)	0.7041916(13)	0.4843789(45)	0.7041883(19)
5.98	1.70256818	0.4884099(39)	0.7070003(19)	0.4883825(35)	0.7069880(15)
6.00	1.70535029	0.4911005(118)	0.7088537(50)	0.4909663(38)	0.7087977(14)
6.01	1.70671610	0.4924924(104)	0.7097962(43)	0.4922291(37)	0.7096838(15)
6.02	1.70806552	0.4938053(64)	0.7107011(32)	0.4934718(30)	0.7105575(13)
6.03	1.70939887	0.4950807(40)	0.7115881(16)	0.4947043(36)	0.7114232(17)
6.04	1.71071646	0.4963132(30)	0.7124510(16)	0.4959199(32)	0.7122791(13)
6.07	1.71457763	0.4998634(27)	0.7149595(10)	0.4994891(31)	0.7147889(15)
6.08	1.71583512	0.5010194(19)	0.7157747(6)	0.5006575(31)	0.7156082(13)
6.10	1.71830738	0.5032879(22)	0.7173807(10)	0.5029551(29)	0.7172208(13)
6.15	1.72425080	0.5087787(26)	0.7212576(10)	0.5085106(19)	0.7211154(12)
6.20	1.72987892	0.5140368(26)	0.7249549(12)	0.5138372(20)	0.7248368(8)
6.30	1.74029271	0.5240287(21)	0.7319188(8)	0.5239220(23)	0.7318284(10)
6.40	1.74972820	0.5334259(25)	0.7383798(11)	0.5333873(23)	0.7383125(9)
6.60	1.76621035	0.5508062(15)	0.7501014(7)	0.5508372(22)	0.7500563(9)
6.80	1.78017964	0.5666348(15)	0.7605281(6)	0.5667010(21)	0.7604924(9)
7.00	1.79221720	0.5811933(20)	0.7699251(8)	0.5812721(12)	0.7698933(6)
7.20	1.80273290	0.5946688(17)	0.7784726(9)	0.5947568(18)	0.7784435(8)

TABLE V. Plaquette expectation values on  $24^3 \times 12$  and  $24^3 \times 48$  lattices with  $\xi = 2$ .

$\beta$	lattice	$N_{opt}$	# of conf.
5.7	$16^3 \times 32$	3	800
5.8	$16^3 \times 32$	5	800
5.9	$16^3 \times 32$	6	800
6.0	$16^3 \times 32$	8	600
	$24^3 \times 48$	8	100
6.1	$16^3 \times 32$	10	400
6.3	$16^3 \times 32$	16	300
	$24^3 \times 48$	20	100
6.5	$24^3 \times 48$	30	100

TABLE VI. Simulation parameters for static quark potential at zero temperature.

$\beta$	lattice	$a_s\sqrt{\sigma}$	$L_s[\text{fm}]$	$\hat{T}$	$\hat{R}_{min}$	$V_0$	$e$	$l$	$\chi^2/N_{DF}$
5.7	$16^3 \times 32^*$	0.4794(66)	3.49	5	$\sqrt{5}$	0.677(36)	0.305(50)	0.934(122)	5.81
5.8	$16^3 \times 32^*$	0.3804(24)	2.77	6	$\sqrt{5}$	0.720(11)	0.326(16)	0.647(49)	3.07
5.9	$16^3 \times 32^*$	0.3190(18)	2.32	7	$\sqrt{5}$	0.688(7)	0.284(11)	0.501(43)	3.20
6.0	$16^3 \times 32$	0.2667(21)	1.94	8	$\sqrt{6}$	0.685(8)	0.283(14)	0.396(73)	0.93
	$24^3 \times 48^*$	0.2611(31)	2.85	8	$\sqrt{6}$	0.699(11)	0.310(19)	0.565(82)	2.05
6.1	$16^3 \times 32^*$	0.2224(20)	1.61	8	$2\sqrt{2}$	0.686(6)	0.297(13)	0.375(61)	1.97
6.3	$16^3 \times 32$	0.1656(19)	1.20	9	$\sqrt{6}$	0.653(5)	0.281(9)	0.239(67)	0.95
	$24^3 \times 48^*$	0.1661(20)	1.81	9	$\sqrt{6}$	0.657(5)	0.294(9)	0.323(68)	1.72
6.5	$24^3 \times 48^*$	0.1242(21)	1.35	9	$\sqrt{6}$	0.622(3)	0.279(6)	0.247(47)	1.75

TABLE VII. Results for the potential parameters on  $\xi = 2$  anisotropic lattices with the plaquette action. The spatial lattice size  $L_s$  is computed using  $\sqrt{\sigma} = 440$  MeV.

$N_s^3 \times N_t$	$12^3 \times 8$	$16^3 \times 8$	$24^3 \times 8$	$20^3 \times 10$	$24^3 \times 12$
$\beta_c(N_t, N_s)$	5.79037(40)	5.79081(54)	5.79138(31)	5.90494(92)	6.00464(67)
$\beta_c(N_t, \infty)$		5.79149(34)		5.90543(116)	6.00512(91)
$T_c/\sqrt{\sigma}$		0.6402(39)		0.6392(39)	0.6364(75)

TABLE VIII. Critical coupling and temperature on anisotropic  $\xi = 2$  lattices. Results for  $T_c/\sqrt{\sigma}$  are obtained in the thermodynamic limit.

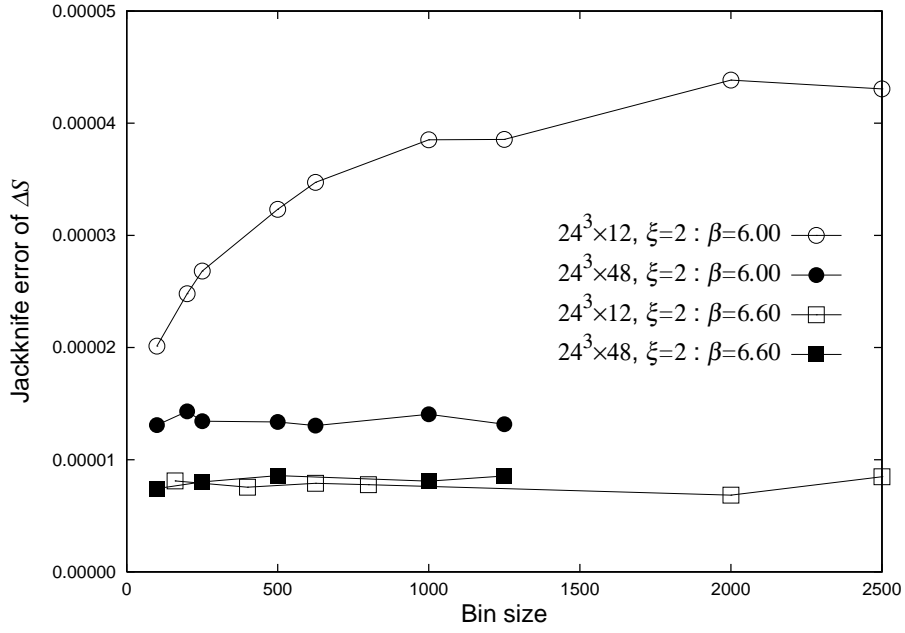


FIG. 1. Typical bin size dependence of jack-knife errors for  $\Delta S$ .

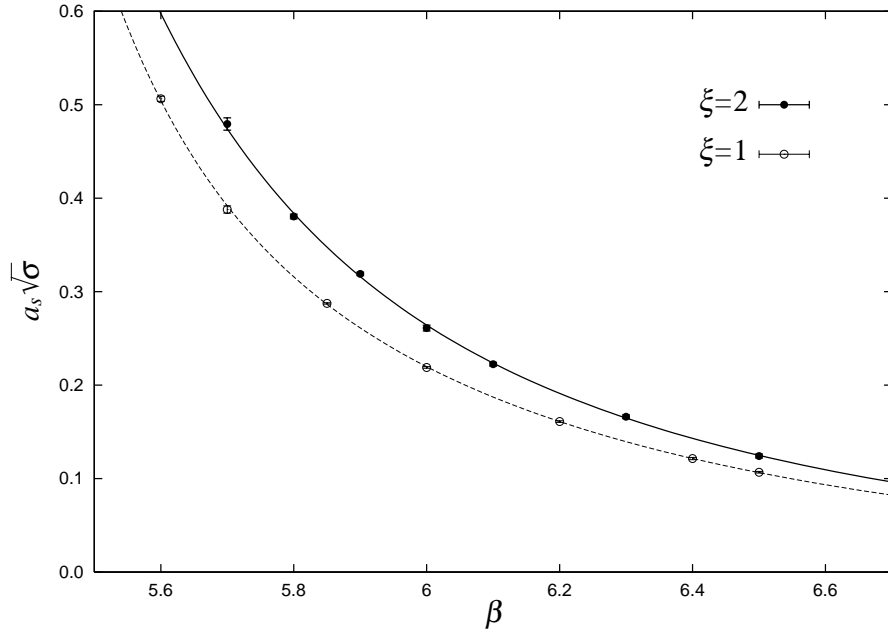


FIG. 2. String tension  $\sigma$  on  $\xi = 2$  anisotropic lattices as a function of  $\beta$ . Scaling fits are based on the ansatz (12).

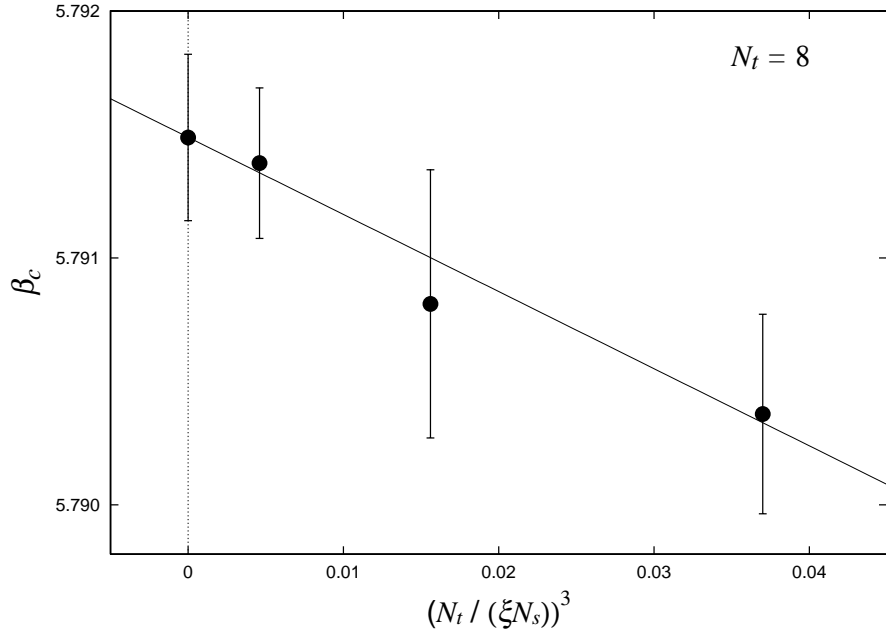


FIG. 3. Finite-size scaling of  $\beta_c$  for  $N_t/\xi = 4$  on  $\xi = 2$  anisotropic lattices.

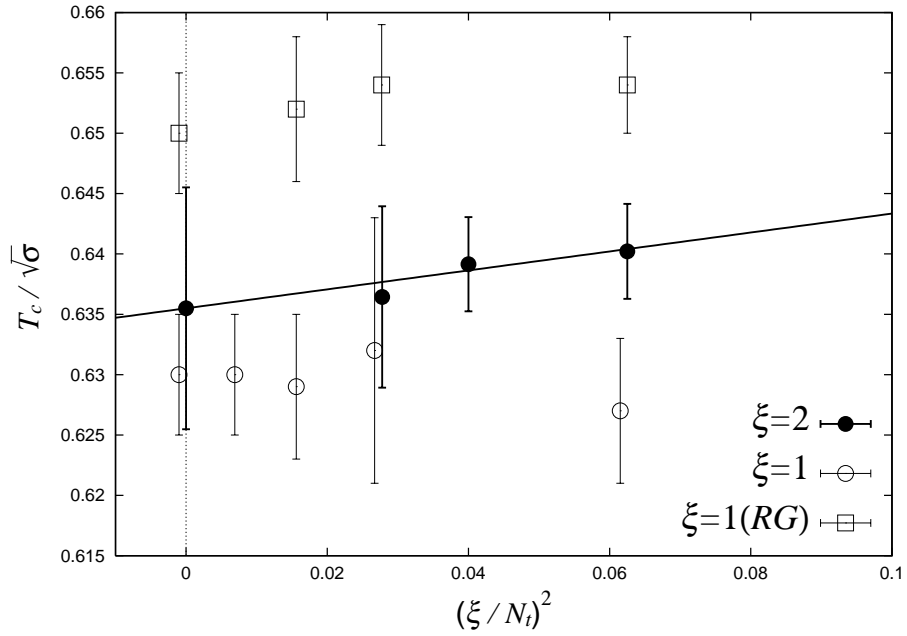


FIG. 4. Critical temperature  $T_c/\sqrt{\sigma}$  on isotropic and  $\xi = 2$  anisotropic lattices.

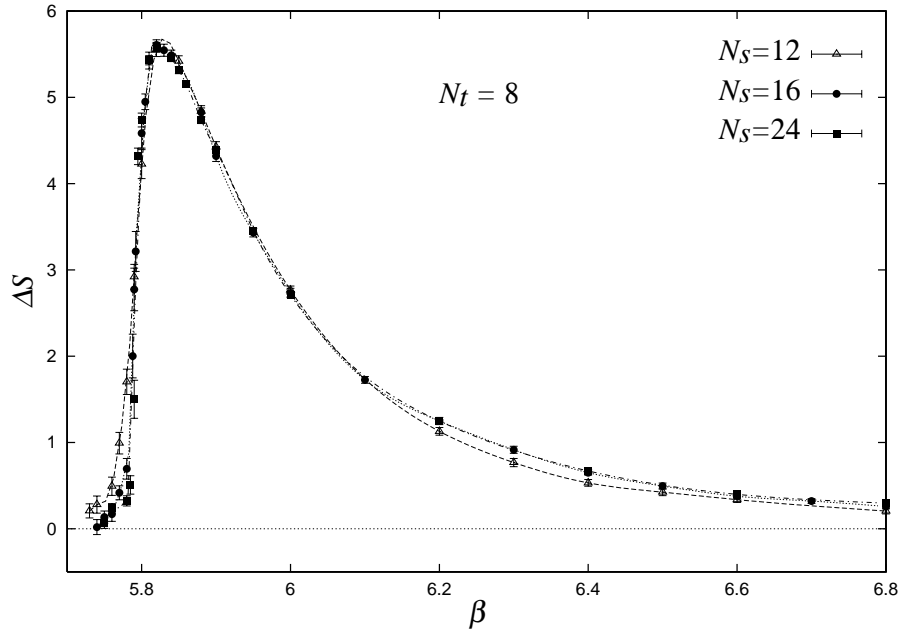


FIG. 5. Spatial lattice volume dependence in  $\Delta S$  at  $N_t/\xi = 4$  on  $N_s = 12, 16$  and  $24$  lattices with  $\xi = 2$ .

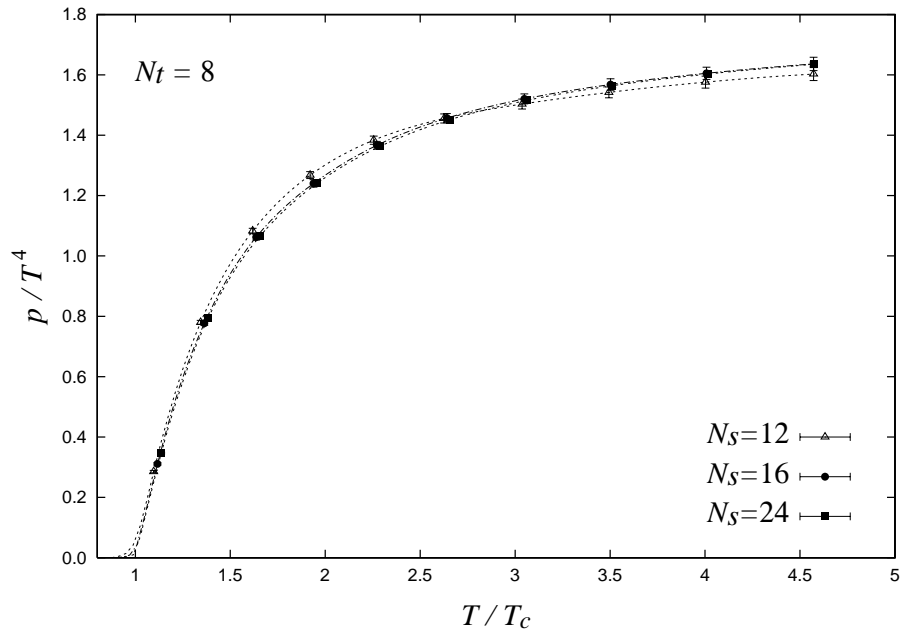
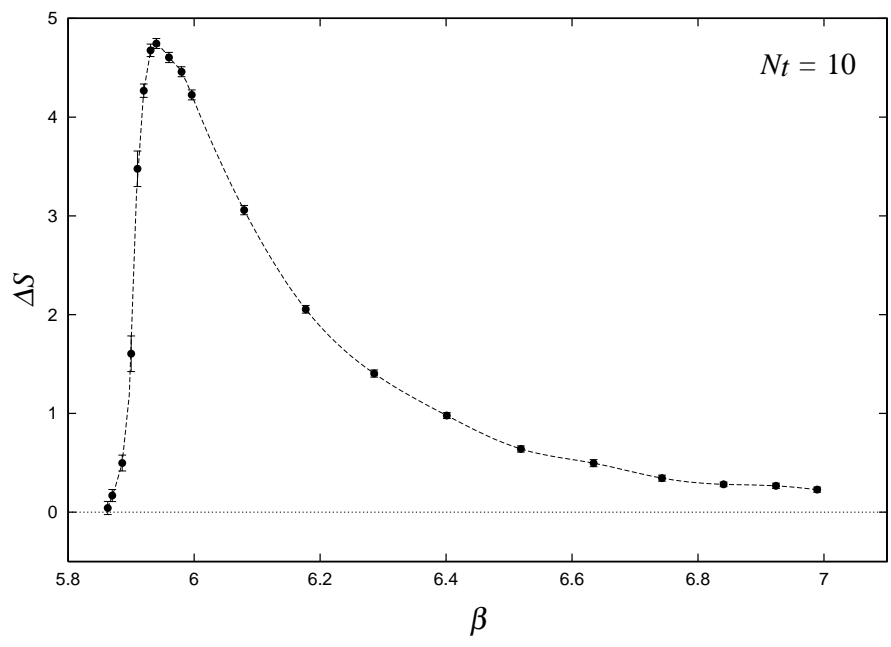
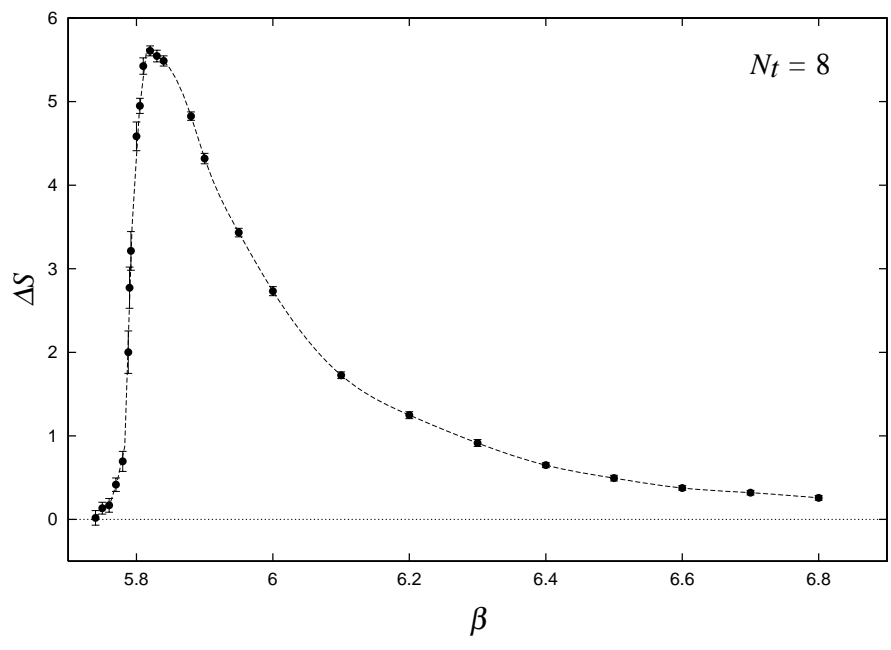


FIG. 6. Spatial volume dependence of the pressure  $p/T^4$  on  $\xi = 2$  anisotropic lattices with  $N_t/\xi = 4$ .





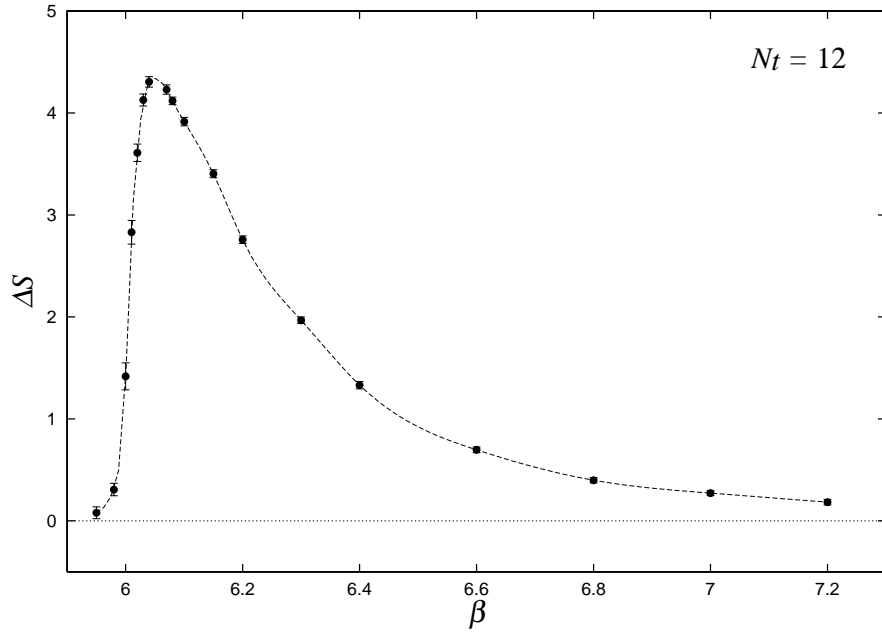


FIG. 7.  $\Delta S$  on  $N_t/\xi = 4, 5$  and  $6$  lattices with  $\xi = 2$ .

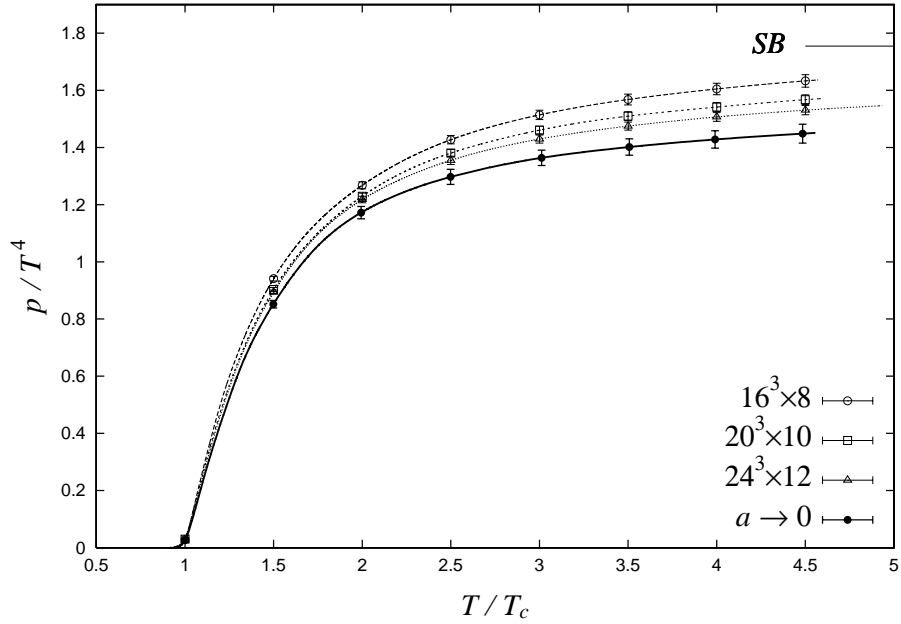
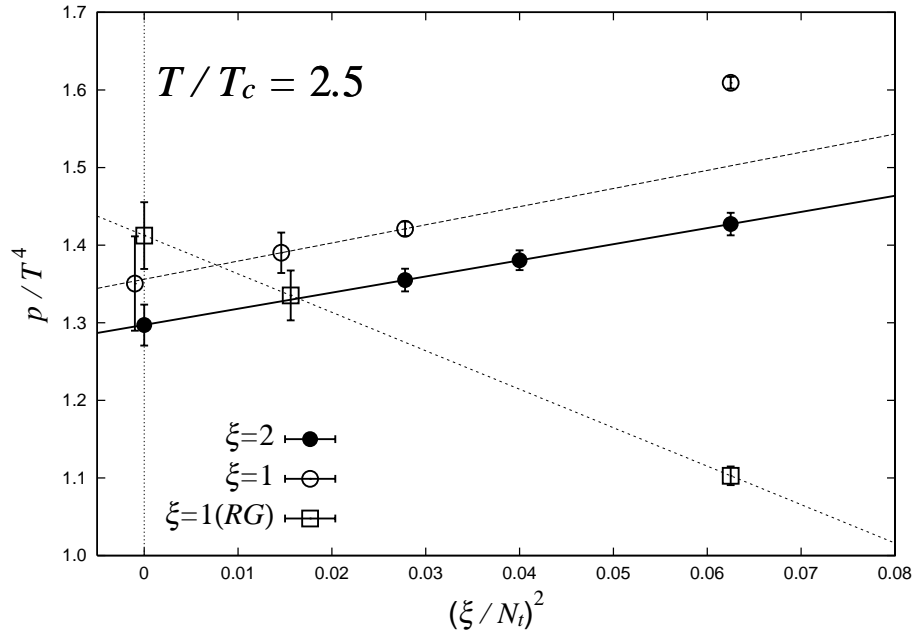
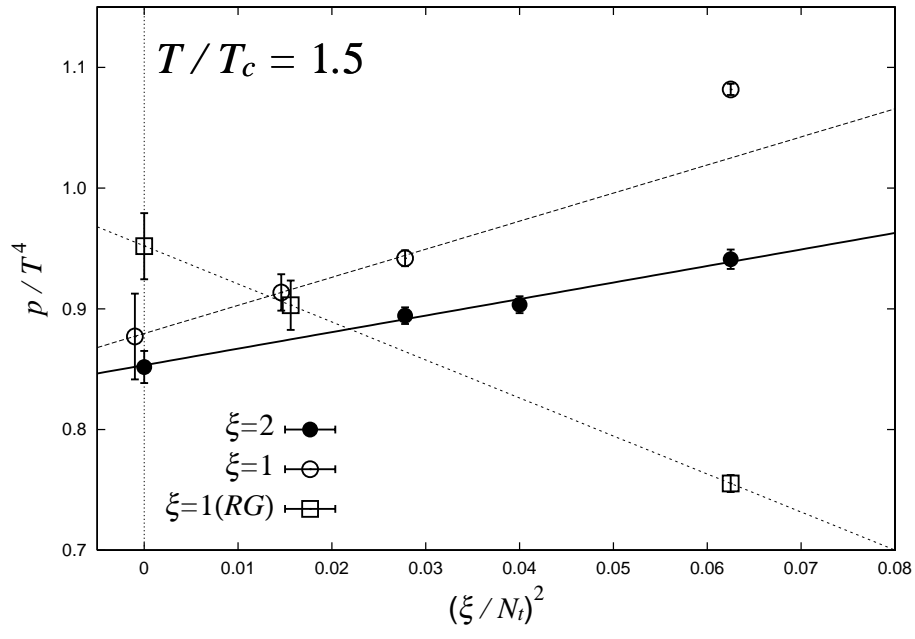


FIG. 8. Pressure  $p/T^4$  on  $\xi = 2$  anisotropic lattices.



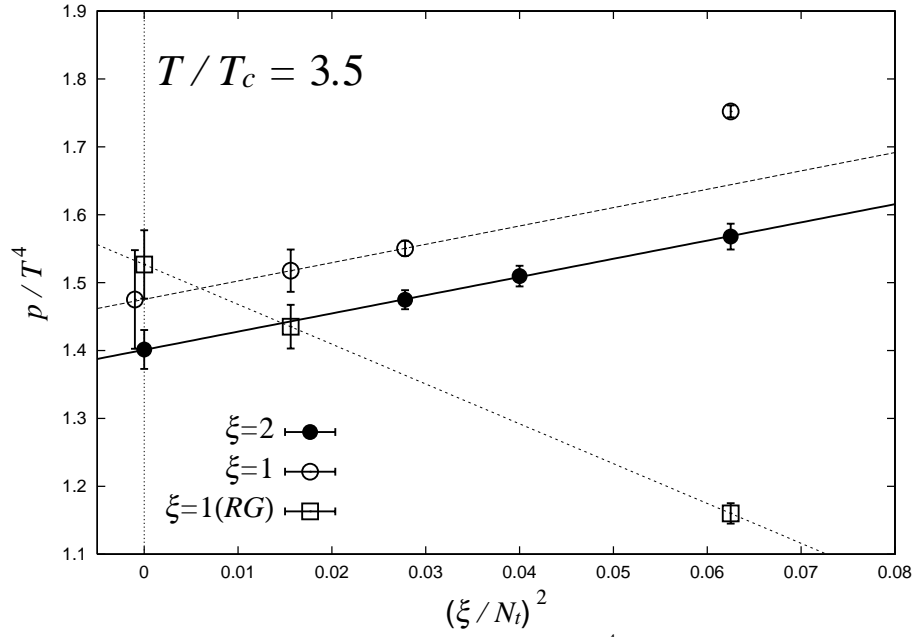


FIG. 9. Continuum extrapolation of the pressure  $p/T^4$  at  $T/T_c = 1.5, 2.5$  and  $3.5$ .

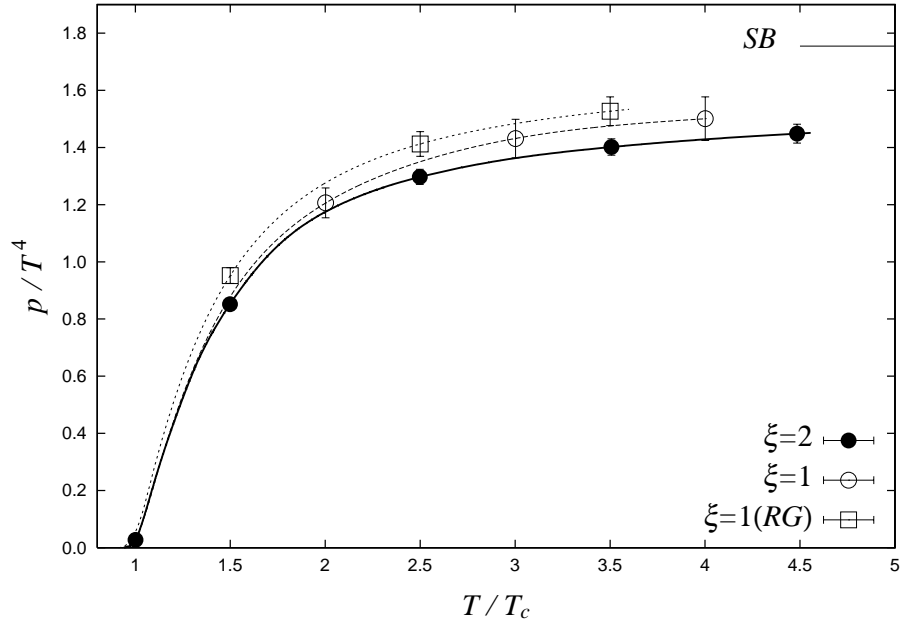


FIG. 10. Pressure  $p/T^4$  in the continuum limit.

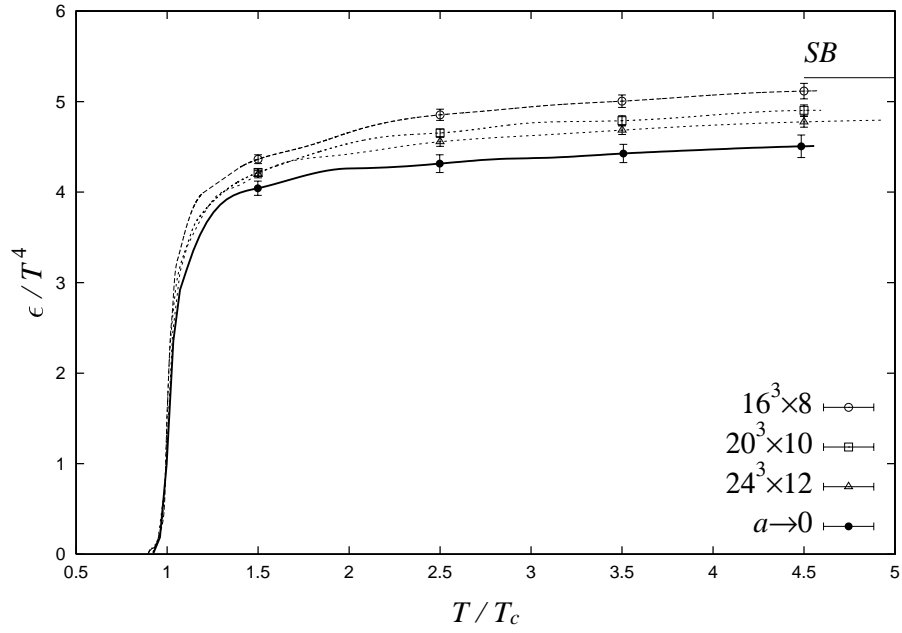


FIG. 11.  $\epsilon/T^4$  on anisotropic  $16^3 \times 8$ ,  $20^3 \times 10$  and  $24^3 \times 12$  lattices with  $\xi = 2$ .

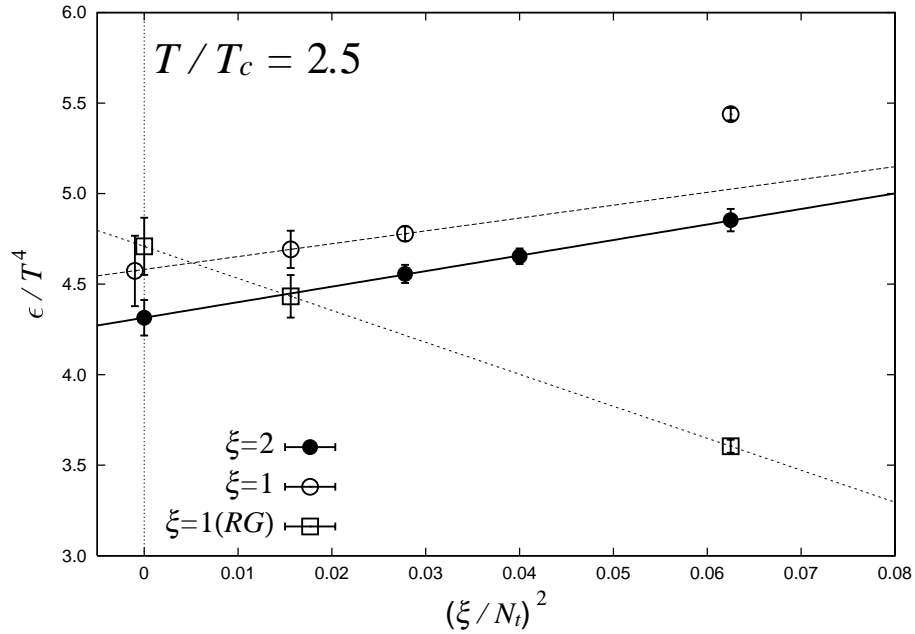


FIG. 12. Continuum extrapolation of the energy density  $\epsilon/T^4$  at  $T = 2.5T_c$ .

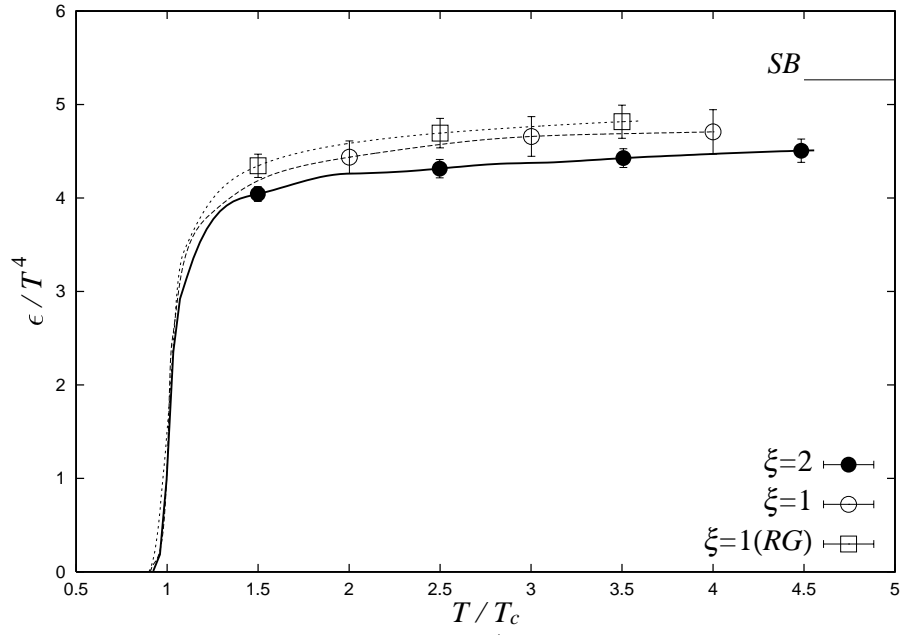


FIG. 13. Energy density  $\epsilon/T^4$  in the continuum limit.